N82 22714

A CONTRIBUTION TO THE AVAILABILITY OF LUNAR RESOURCES FOR POWERSAT CONSTRUCTION

T. A. Heppenheimer
Center for Space Science
Fountain Valley, California

A number of authors have discussed the use of lunar resources in powersat construction, wherein these resources are to be transported with the aid of a lunar mass-driver. Previous contributions by the present author have included studies of achromatic trajectories and of the mass-catcher and associated transfer trajectories to a space manufacturing facility. An important problem, heretofore essentially untreated, is the minimization of cross-track errors in the launch of payloads by mass-driver. This problem is important because an error $\Delta\dot{y} = 1$ cm/sec (normal to the lunar surface) produces a miss of 500 meters, for a catcher near the L_2 libration point. If the error is $\Delta\dot{z} = 1$ cm/sec, parallel to the lunar surface, the miss is 30 meters.

Figure 1 gives a block diagram of the mass-driver; Figures 2 and 3 indicate the technology which is applied. The proposed mass-driver buckets or payload-carriers employ the design concepts of Chilton, Kolm and associates, as developed in 1976. In Fig. 2, the new feature is the payload constraint/release system. The payload is conceived as a triaxial ellipsoid having axes in the approximate ratio 0.95:1.00:1.05, with mass 20 kg, and consequently with mean diameter 25 cm. It is of unprocessed lunar soil and is contained within a bag woven from lunar-derived fiberglass, as proposed by Criswell, the fiberglass being prepared at the lunar base. In addition, the payload is flashed with a thin coating of metallic aluminum, to make its surface electrically conducting. The payload housing then is a double hemiellipsoid, moulded to the reference payload shape. The rear housing half is strongly braced and secured. The forward half fits tightly against the rear half during bucket acceleration (at 1000 m/sec^2).

Passive magnetic damping: Following the main acceleration phase is a section of mass-driver track which is precision aligned; the optical alignment system used in the Stanford Linear Accelerator appears applicable. This section, up to several kilometers in length, gives a very smooth bucket motion wherein preexisting bucket oscillations may die out. Chilton et. al. give reference oscillation frequencies as 28 Hz laterally, 20 Hz vertically. Figure 4 illustrates a novel means for damping: electromagnetic fins.

The phenomena of magnetic damping is well-known: if a conducting loop oscillates within a transverse magnetic field, then by Lenz' law there arise eddy currents within the loop, the decay of which absorb energy at the expense of the oscillation. In the present instance, each of the cruciform fins of Fig. 4 has associated a conductor carrying current I, parallel to the fin length L and separated by clearance C. Fin width is W and resistance of the fin is R;

$$R = 2\rho(L + W)/A_x \qquad (1)$$

where ρ is resistivity in ohm-meters, A_x is conductor cross-sectional area. D.J. Ross has given the equation of motion of a bucket undergoing lateral oscillations which are damped using electromagnetic fins:

$$\ddot{\xi} + \frac{2}{Rm}\left(\frac{\mu_0 ILW}{2\pi C(C+W)}\right)^2 \dot{\xi} + \frac{k}{m}\xi = 0 \qquad (2)$$

ξ is y or z; m, bucket mass taken as 40 kg; k, spring constant taken as 12.6×10^5 newton/meter for $\xi = z$ and 6.3×10^5 for $\xi = y$, following Chilton et. al. If L =

1 meter, W = 32 cm, A_x = 4 cm^2, C = 4 cm and the fins are of copper then R = 1.138×10^{-4} ohm and critical damping is achieved for I = 2.022×10^5 amperes when ξ = z, or I = 1.700×10^5 amps when ξ = y.

Two other events occur during passive damping. The track twists or corkscrews to give the bucket a rotation 0.1 rad/sec about the x-axis. Also a trimming acceleration is applied to adjust bucket velocity to a desired value.

Separation and snapout: Figure 5 illustrates the means whereby the payload is separated from the bucket. High launch accelerations will have wedged the payload tightly in the housing; the "wrenchout" is an abrupt deceleration applied to the bucket by track electromagnetics, causing the payload to wrench free. The forward half of the payload housing is supported by a telescoping boom, which collapses forward, receiving the payload in a compliant fashion. A step-function acceleration-deceleration translates the bucket forward with respect to the payload, providing clearance. Then the bucket undergoes snapout: a sudden lateral translation which leaves the payload free in space.

Snapout is accomplished with zero lateral perturbation on the payload from interaction of bucket magnetics with fine-grained iron in the payload material. It is assumed that magnetic field strength B is always sufficient to saturate the iron to its maximum magnetic moment. Then the perturbation $\dot{z} \propto \int (dB/dz)\, dt$ which is driven to zero by considering that with the bucket magnetics of Fig. 2, dB/dz shifts from positive to negative with increasing z (distance above bucket midplane). When $\dot{z}$ = 0, bucket passes behind a mu-metal barrier for isolation.

Downrange correction: Figure 6 illustrates the scanner, lateral corrector, and overall system for correction. The payload shape is a triaxial ellipsoid:

$$Ax^2 + By^2 + Cz^2 + 2Dxy + 2Exz + 2Fyz + Gx + Hy + Iz + 1 + 0 \qquad (3)$$

The nine coefficients specify payload semi-axes, orientation in space, and position of the center of figure. Six lasers, arranged as shown on an octagon, are interrupted by the payload in flight; the timed interruptions serve to determine all nine coefficients. The center of figure, however, is at distance d from the center of mass and the latter is to be determined. Three sequential determinations of the coefficients of eq. (3) allow specification of the rotation axis; so we first find the axis of the rotation applied during passive damping. We then torque the payload in the z-direction, to give a rotation component $\omega_z \sim \omega_x$ = 0.1 rad/sec; this torque involves a bias motion $\dot{z} = 0.4\,(a/d)\,a\omega_z$; a is payload mean radius. Then three sequential scans determine the new rotation axis; its intersection with the old axis given the center of mass.

The corrector is a cylindrical array of conductors, any of which may be charged to simulate a line of charge acting on a conducting sphere (the payload). The resulting force has magnitude

$$F = \frac{\lambda^2}{\pi\varepsilon_o}\left(1 - (a/R)\right)^{-\frac{1}{2}} \cdot (a/R)^2 \sin^{-1}(a/R) \quad \text{newtons} \qquad (4)$$

where R is distance from sphere center to the line charge, λ line charge magnitude in coulombs/meter. Each line charge is regarded as produced by a cylinder of radius r; within the corrector, these cylinders (conductors) have mutual centerline separation b. Hence the capacitance of such a conductor is

$$C = \lambda/V = 2\pi\varepsilon_o / \{\cosh^{-1}\left((b^2 - 2r^2)/2r^2\right)\} \qquad (5)$$

Voltages $V \sim 10^6$ volts suffice. Thus, lateral dispersions can be reduced so as to permit aim within a 3-meter circle at L_2, for 0.1-cm tracking accuracy.

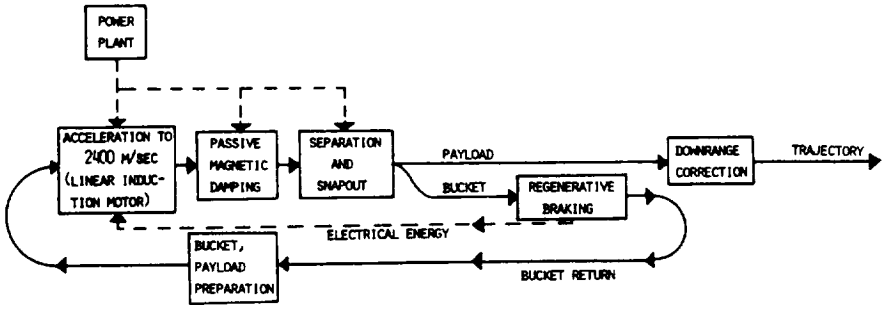

Figure 1. Block diagram of lunar mass-driver for launching of lunar materials at $>10^6$ tons/year. (Modified from Chilton et. al., AIAA Progress Series, Vol. 57, 1977, p. 40)

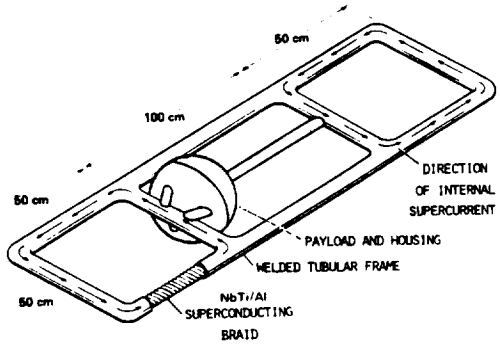

Figure 2. Mass-driver bucket. Frame is cut away to show superconducting braid. Note payload constraint/release system. (Modified from Chilton et. al., op. cit., p. 50)

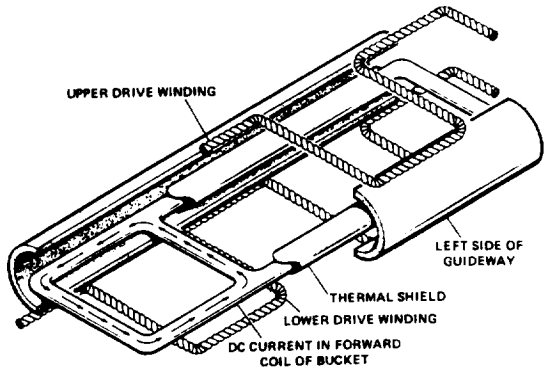

Figure 3. Mass-driver geometry. A portion of the drive windings for one of three phases is shown. Forward portion of bucket superconducting loop appears with thermal shield removed. Payload and support not shown. (After Chilton et. al., op. cit., p. 42)

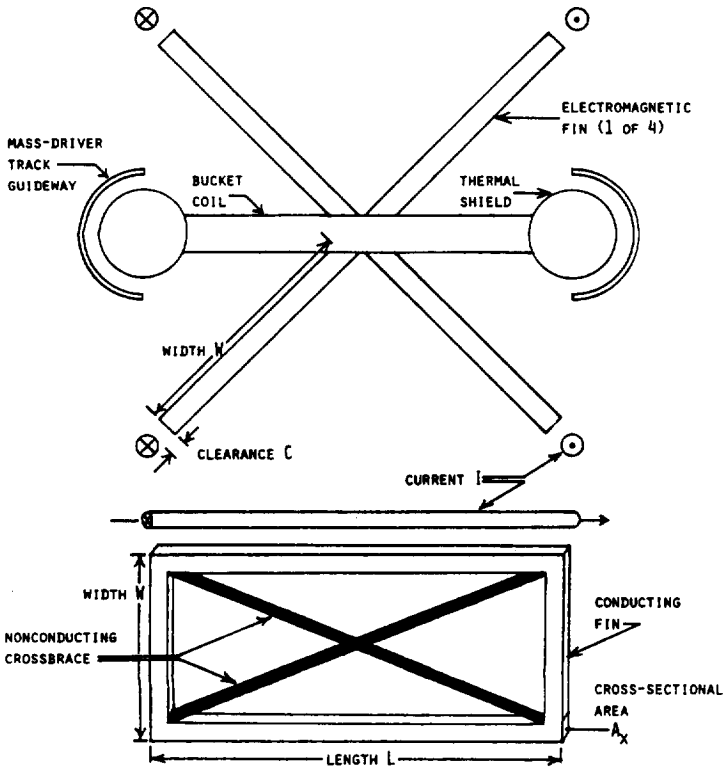

Figure 4. Electromagnetic fins for passive magnetic damping of bucket oscillations. Top, bucket is shown in end view with payload and restraint removed. Bucket oscillatory motions (resolvable into cruciform components) induce eddy currents in fins owing to adjacent currents I, thus damping these motions. Bottom, mechanical design of fin as a crossbraced rectangular conductor. Note that adoption of this concept will force redesign of the mass-driver/bucket concept of Figs. 2, 3.

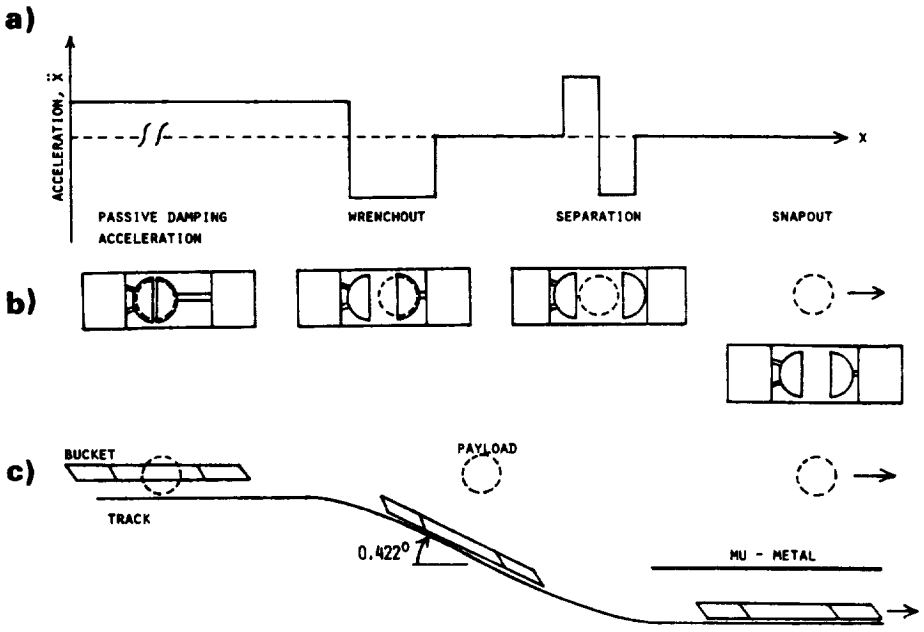

Figure 5. Separation and snapout. (a) Acceleration on bucket, $\ddot{x}$, as schematic function of along-track distance x. (b) Separation of payload from bucket; see text for discussion. (c) Detail of snapout; note mu-metal barrier.

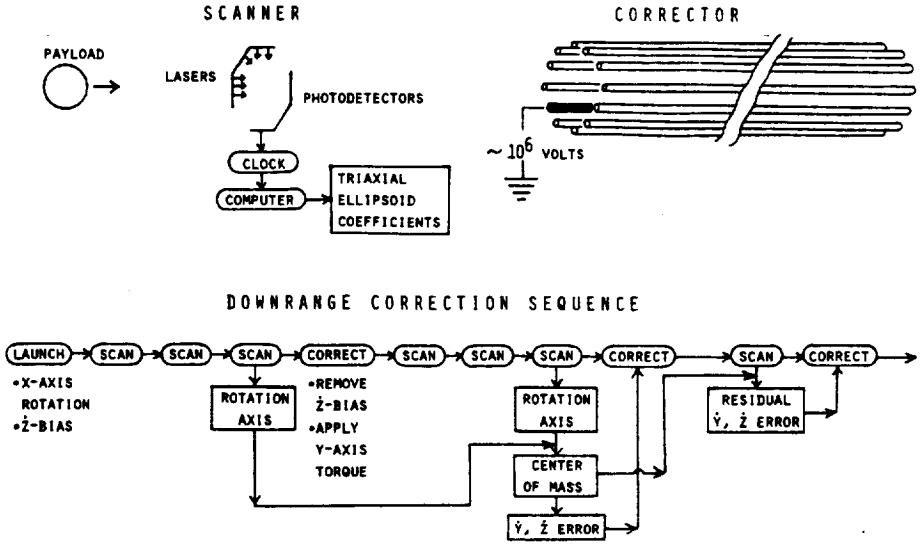

Figure 6. Downrange correction. Scanner employs six lasers plus timed photodetectors to determine payload location, dimensions, and orientation. Corrector charges a selected conductor within an array for electrostatic deflection of payload; payload is electrically neutral but conductor induces a charge redistribution. Correction sequence determines initial rotation axis, applies a lateral torque to payload, then redetermines rotation axis, thus yielding payload mass center location. Thereafter observed payload lateral position errors are interpreted as due to lateral velocity components of center of mass, which are electrostatically corrected. Final scan/correction steps occur atop a mountain some 75 kilometers (30 seconds flight time) downrange from launch site.